Supplementary Information :

Direct measurement of the electronic spin diffusion length in a fully functional organic spin valve by low energy muon spin rotation

---

Section 1: Characterisation & Additional Measurements

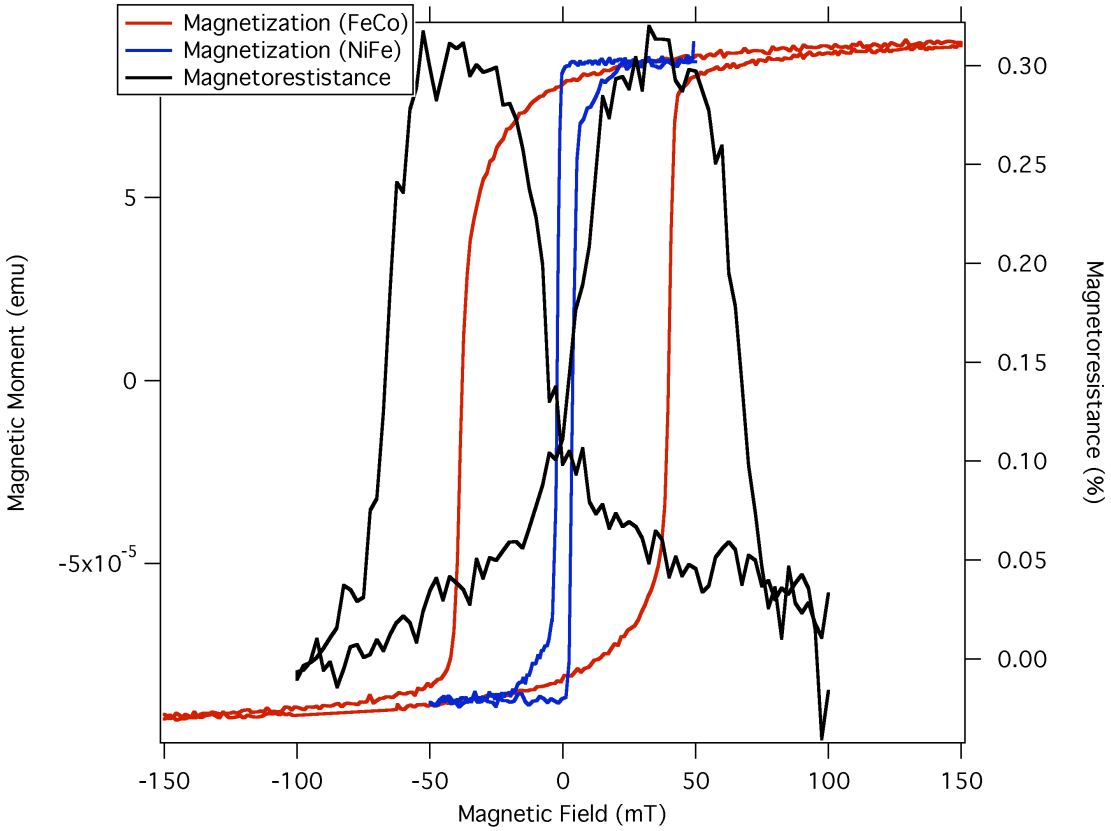

Figure 1.1: Magnetisation measurements for our two electrodes ($Ni_{81}Fe_{19}$ blue; $Fe_{50}Co_{50}$ red) plotted on the same graph as the magnetoresistance from our spin valve (black). The NiFe moment has been scaled by a factor of two. Even though the magnetisation of both FM layers is at least 95% switched, it is clear that the MR remains high, indicating that the spin polarisation remains relatively unchanged. This is due to the nature of the switching of magnetisation in FM electrodes. Whilst the bulk of the NiFe layer's magnetisation switches in a 5mT field, it is the interface from which we inject and the magnetisation at the interface remains pinned to the roughness.

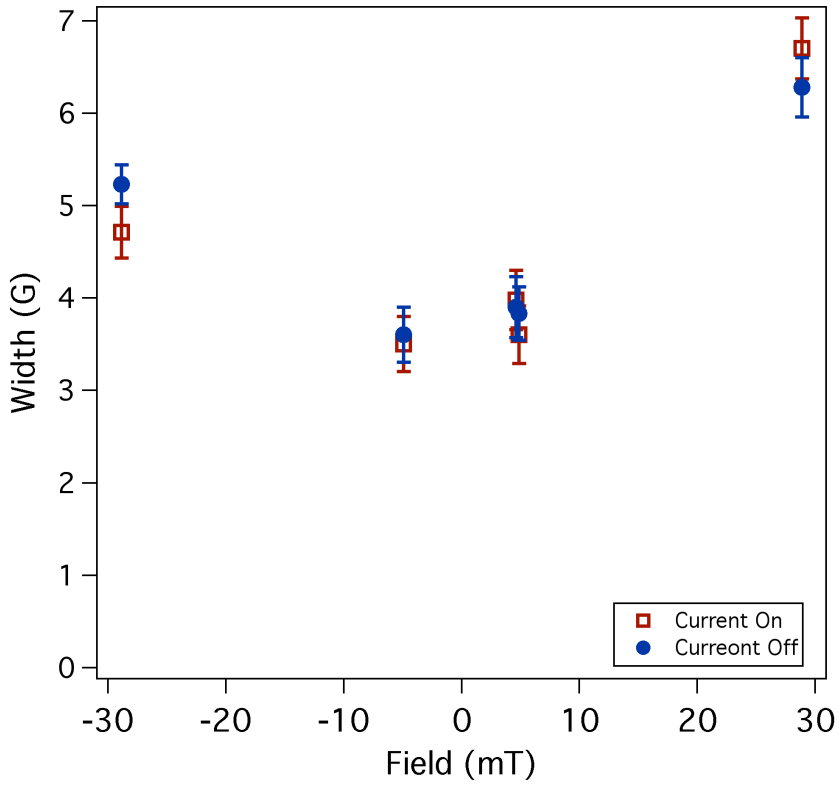

Figure 1.2: The half-width half maximum of the skewed Lorentzian (γ in Equation 2.4 of this document) fitted to our 6.23 keV data. The change in skewness for the same data/fits is plotted in Figure 3 of the main paper. It is clear that the width is the same (within the error bars) for both current states.

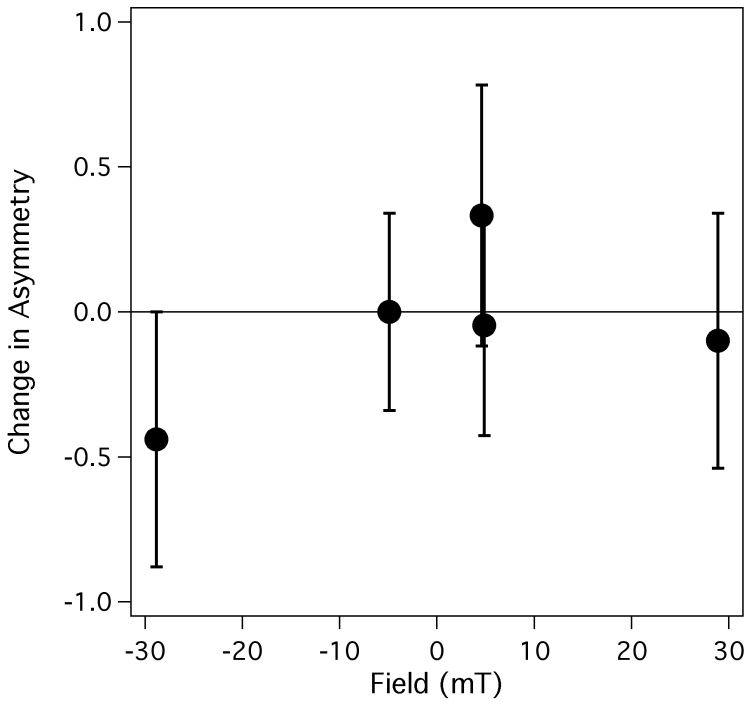

Figure 1.3: The difference of current on and off asymmetry (A_0 in Equation 2.4 of this document) fitted to our 6.23 keV data. The change in skewness for the same data/fits is plotted in Figure 3 of the main paper. It is clear that there is no difference between current on and off (within the error bars).

Section 2: Time domain analysis

Positive muons decay to a positron, muon antineutrino and electron neutrino. The angular emission of positrons is well characterised, with the emission direction being correlated with the muon's spin at time of decay. Thus, by measuring the direction and the timing of a statistically significant number of decay positrons it is possible to follow directly the evolution of the muon's spin ensemble as a function of time after implantation. This allows a wealth of information to be gained about the host material in which the 100% spin polarised muons are implanted and come to rest. They can act as passive local magnetic microprobes, for example directly measuring magnetic field distribution at the implanted site with very high sensitivity (less than 0.1 mT). Being able to follow the evolution of the spin with time means that the magnetic field experienced by the muon can be determined through the measurement of the Larmor precession of the muon spin. In a magnetic field the spin will precess about the field direction with a frequency ω_μ proportional to the field B

$$\omega_\mu = \gamma_\mu B \qquad (2.1)$$

where $\gamma_\mu/2\pi$=135.5 MHz T^{-1} is the gyromagnetic ratio for the muon.

The spin rotation can be observed using two positron counters, a and b, mounted on the opposite sides of the sample. The number of positrons detected by each counter as a function of time ($H^a(t)$ and $H^b(t)$) reflects the time dependence of the muon spin polarisation along the axis of observation defined by the two detectors:

$$H^a(t) = N_0^a \cdot \exp\left(-t^a/\tau_\mu\right) \cdot \left[1 + A^a(t)\right] + C^a \qquad (2.2)$$

$$H^b(t) = N_0^b \cdot \exp\left(-t^b/\tau_\mu\right) \cdot \left[1 + A^b(t)\right] + C^b \qquad (2.3)$$

where $N_0^{a,b}$ is the initial counts at zero time, τ_μ~2.2μs is the muon's lifetime, $C^{a,b}$ is the time independent background and the asymmetry $A^{a,b}(t)$. The asymmetry contains all

of the information about the time evolution of the muon's spin polarisation.

We initially fitted our data to a skewed Lorentzian, such that $A^i(t)$ is given by

$$A^i(t) = \sum_j \left(\frac{A_0}{\left(1 + \left((B^j - B_0)/(\gamma(1 \pm \Delta))\right)^2\right)} \right) \cdot \cos(\gamma_\mu B^j t + \phi^i), \qquad (2.4)$$

where A_0 is the asymmetry, γ is the half-width half maximum, Δ is the skewness parameter (Δ is added to or subtracted from γ depending on whether $B \geq B_0$ or $B < B_0$), B^j is the local magnetic field and is an array of evenly spaced fields spanning ±7 linewidths, B_0 is the mean magnetic field, t the time and ϕ^i the phase of detector i. This function is appropriate to extract trends and to provide an overview of the data.

In order to extract the spin diffusion length, we fitted the asymmetry for all energies and detectors to an identical function, where the only difference was the weighting of the individual stopping profiles. The asymmetry is given by

$$A^i(t) = A_0 \left((1-p) \cdot \cos\left(2\pi B_a t + \phi^i\right) + p \cdot \sum_z n(z,E) \cdot \cos\left(2\pi B(z) t + \phi^i\right) \right) \qquad (2.5)$$

where $n(z,E)$ is the normalised stopping probability at a depth z for a given energy E, the first term describes the non-relaxing oscillatory background resulting from $(1-p)$ muons missing the sample (the muons precess around the applied magnetic field) and the magnetic field inside the organic spacer is given by

$$B(z) = B_{d1} \cdot \exp\left(-z/\lambda_{d1}\right) + B_{d2} \cdot \exp\left(-(d-z)/\lambda_{d2}\right) + B_s \cdot \exp\left(-z/\lambda_s\right) + B_a \qquad (2.6)$$

where B_a is the applied field, B_{d1} is the dipolar field at the top interface with a characteristic length scale of λ_{d1}, B_{d2} is the dipolar field at the bottom interface with a

characteristic length scale of λ_{d2}, d is the organic spacer layer thickness and B_s is the magnetisation induced by injected spins with a characteristic length scales of λ_s.

The muons hitting the top and bottom ferromagnetic electrodes precess at frequencies too great for our setup to measure and do not contribute to the precessing signal. We also assume that the fraction of muons hitting the PTFE blocks for holding the spring contacts also do not contribute to the background, due to muonium formation. These signals simply add to the time independent background and are taken account of in Equations 2.5 and 2.6. Any muons hitting the Ag backing plate add to a non-relaxing oscillating background, with the frequency determined by the applied magnetic field. In order to estimate this non-relaxing oscillatory background fraction, we placed a position sensitive detector at the sample position and measured the distribution of muons that stop on the sample plate for each of the relevant transport energy settings. The non-relaxing oscillatory background is approximately 5% and therefore we fixed p to 0.95 in Equation 2.5.

We note that the two components denoted by d1 and d2 account for the stray fields from the FM layers which are not a function of current. Therefore these parameters have been reliably obtained from the zero-current μSR. In the current off data, B_s was fixed to zero and the contributions from the dipolar fields were fitted (shown in Table 2.1). In the current on data, the parameters obtained for the dipolar fields were fixed to these values and the only fitting parameters were thus B_s and λ_s.

Temperature (K)	λ_{d1} (nm)	λ_{d2} (nm)	B_{d1} (mT)	B_{d2} (mT)
10	8 (1)	10 (5)	500 (10)	800 (200)
25	8 (1)	10 (5)	490 (10)	800 (200)
70	7 (1)	10 (5)	490 (10)	800 (200)
90	7 (1)	10 (5)	480 (10)	800 (200)

Table 2.1: Parameters obtained from the fits to the current off μSR spectra. Numbers in brackets represent the statistical error.

Section 3: Sample roughness

Our samples have both correlated and uncorrelated roughness, which play an important role in the dipolar fields and must be explicitly taken account of in the analysis. There are two different length scales of roughness in our sample.

Figure 3.1 shows an AFM image taken of the top NiFe layer of our spin valve, where the roughness has a lateral size distribution of 20 – 100 nm with a maximum to minimum out of plane roughness of 4.5 nm. Taking a histogram of the out of plane height distribution results in approximate Gaussian profile, also shown in Figure 3.1, where the full width at half maxima (FWHM) is approximately 1.5nm. This FWHM is consistent with our specular X-ray measurements performed on a single layer of Alq3 shown in Figure 3.2, from which we are able to extract the thickness, density and out of plane roughness to a high degree of accuracy (these were used in our Monte Carlo calculations for the muon's stopping profile). Assuming a Gaussian profile to the roughness, we have extracted a FWHM of 1.4nm from the X-ray measurements. In Figure 3.3 we plot the specular reflectivity obtained from our spin valve and from the multiple fringes extending to large angles, it is clear the sample has a similar roughness.

A second type of roughness is vertically correlated with a relatively uniform lateral length scale. The lower half of Figure 3.3 shows the off-specular X-ray reflectivity, taken at a detector angle of 1.043 degrees. Whilst specular reflectivity probes Q_z, the wave-vector normal to the surface of the film, off-specular reflectivity probes Q_x, a wave vector parallel to the film surface. It is immediately obvious that there are also interference fringes in the off-specular data, which can only be present if the sample

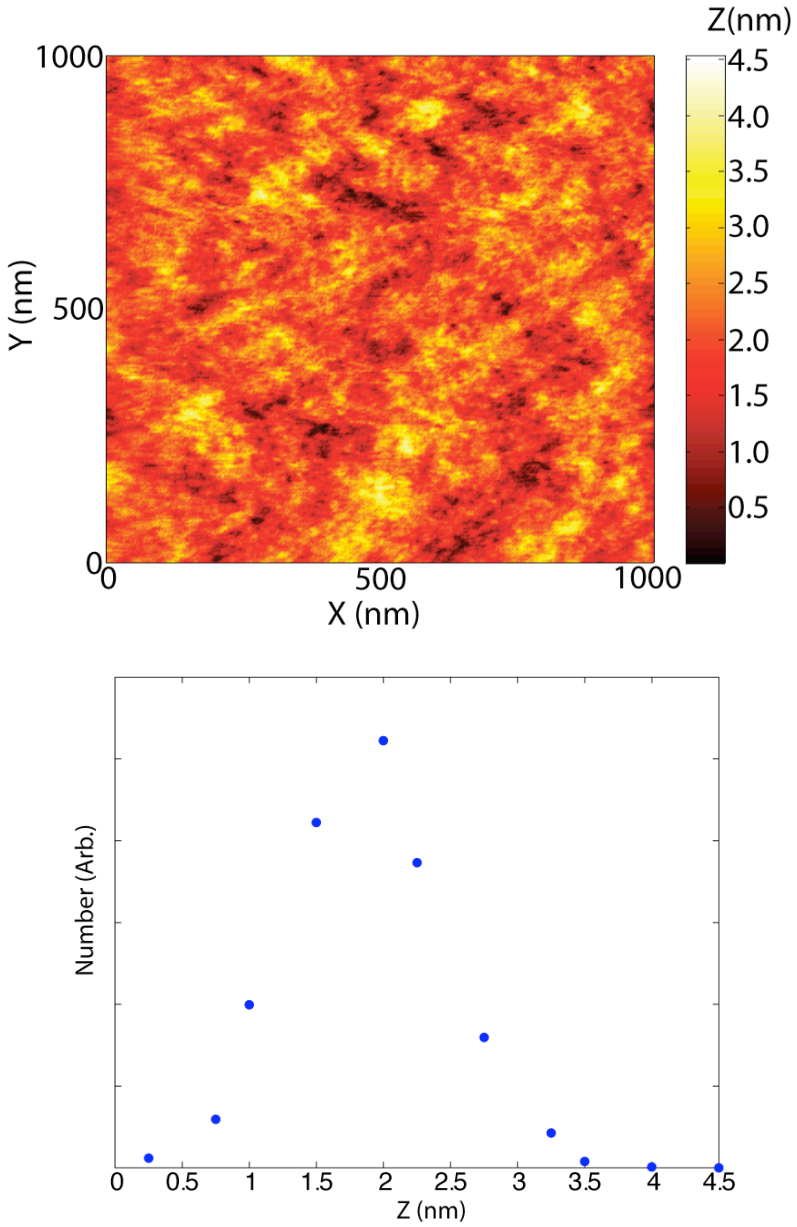

Figure 3.1: Top: A typical AFM image of the top electrode (NiFe) of our spin valves, where it is clear that over the measurement area (1μm x 1μm) the peak-to-peak roughness is 4.5nm. It is possible to see that the lateral "grains" have a size distribution of 20 – 100 nm. Bottom: A histogram of the AFM image shown above, from which we can extract the FWHM roughness to be approximately 1.5nm. This is consistent with the roughness extracted from our X-ray measurements shown in Figure 3.2.

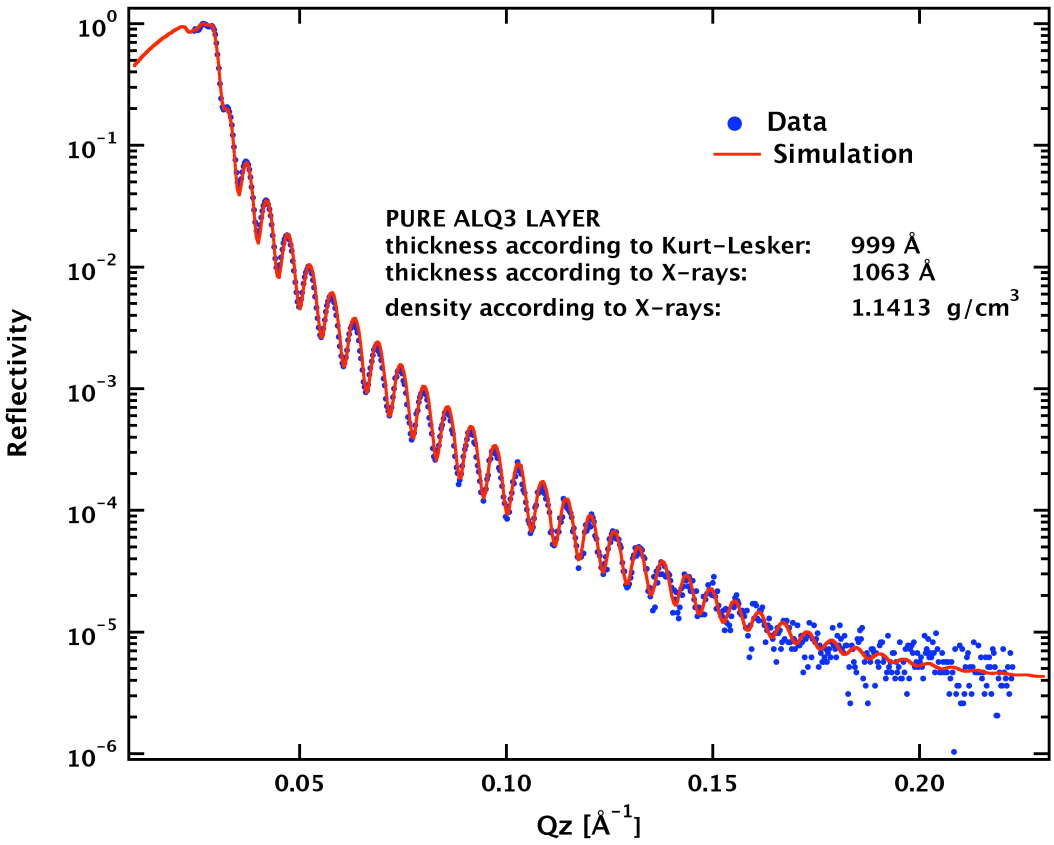

Figure 3.2: X-ray reflectivity for a 100 nm pure Alq_3 film. The data was fitted to an optical transfer matrix model and the layer roughness (1.4 nm) was assumed to have a Gaussian profile. Measurements of individual layers is essential in order to gain accurate thicknesses and densities for our Monte Carlo simulations, as there is considerable complexity in analysing multi-layer reflectivity data.

has correlated vertical roughness with a relatively uniform lateral length scale. Correlated roughness is required to see the Bragg sheet and a uniform lateral length scale is required to see the fringes. It is possible to calculate the lateral length scale from the fringe separation to be 50 μm. Unfortunately it is not possible to perform AFM measurements due to the limited field of view of our setup, although judging from the numerous fringes observed in the specular data out to large angles, the vertical length scale will be relatively small. The source of this roughness could be substrate structure or crystallographic grains in either or both of the FM electrodes, or the organic layer.

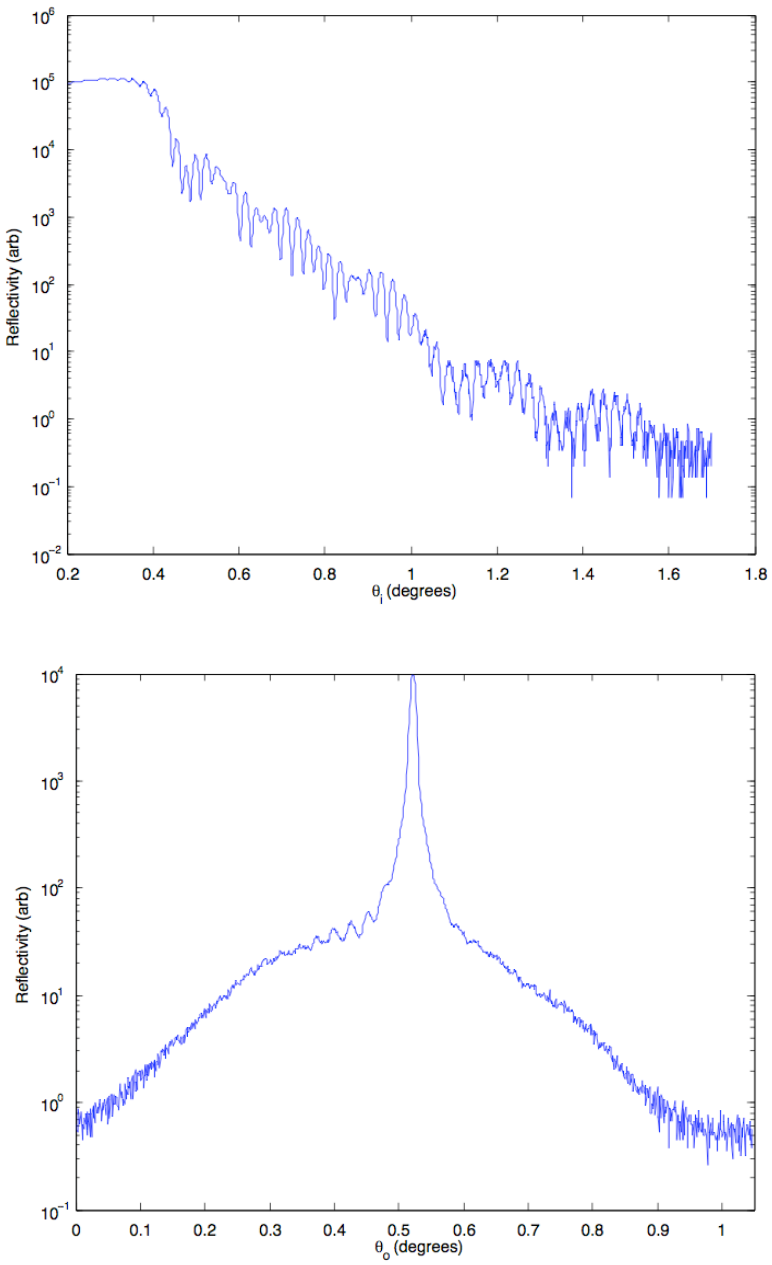

Figure 3.3:Top: Specular X-ray reflectivity data from our spin valve. Bottom: Off-specular X-ray reflectivity data from our spin valve. Fringes on the Bragg sheet are visible (see text). The data has a skewed shape due to the sample illumination changing as it is rotated through the beam. Note that the fringes disappear at large angles. This is due to the X-ray correlation length becoming smaller than the lateral length scale (50μm) as the sample is rotated through the beam.

Section 4: Dipolar Fields

It is clear that the magnetic return fields, or dipolar fields, emanating from the rough ferromagnet are important to the interpretation of the data. To visualise the problem of the correlated roughness, we have plotted in Figure 4.1 a 2D (y and z axis) slice of the magnetic flux density present at a rough interface with a ferromagnet. Note that the muon beam is parallel to the z-axis. We have calculated the flux density by assuming the roughness results in a similar flux density to a series of offset 'bar magnets', forming a series of 'pillars'. This is shown in the schematic diagram in Figure 4.1.

At first, it is evident that the magnetic field is manifestly 'negative' (opposed to the applied magnetic field) at large distances away from the interface. However, close to the interface there are areas of 'positive' (aligned with the applied magnetic field) and 'negative' magnetic fields, which is correlated with the relative position of the pillars (i.e it is positive 'between' the pillars). If the roughness is correlated through the layers (as present to some degree in our sample) as shown in the schematic diagram in Figure 4.1, then an ensemble of muons that stop near the interface, sample both positive and negative magnetic fields. Importantly, the flux density between the pillars (positive) is around an order of magnitude larger than adjacent to the pillars (negative). If the z-component of the roughness is not significantly smaller than the mean penetration of muons into the sample, then the net dipolar fields that the muons experience are in fact *positive*, explaining the positive skewness to our lineshapes (Figure 2 in the main paper). Both of these phenomena can be most readily appreciated by integrating the flux density over the y-direction (but using a more realistic aspect ratio), as shown in Figure 4.2.

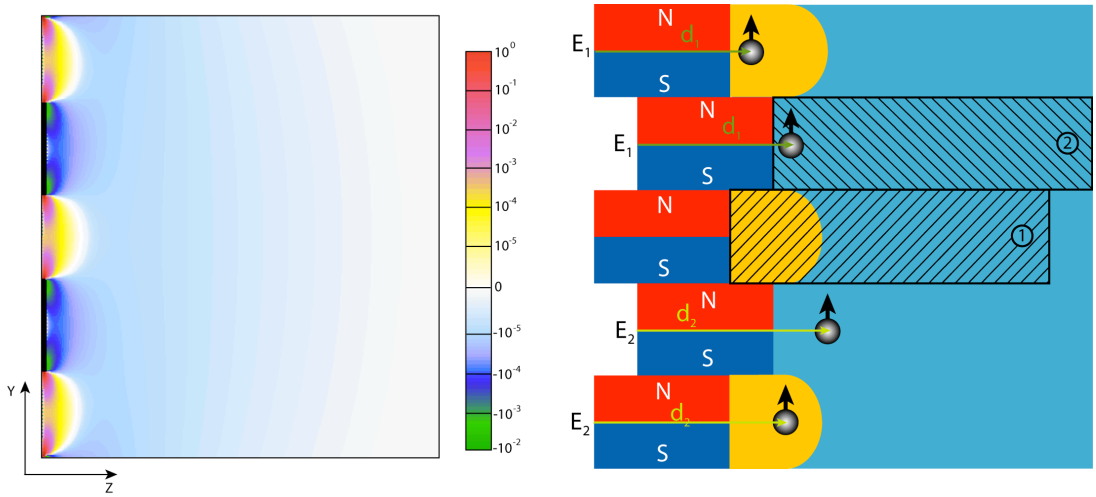

Figure 4.1. Left: the flux density calculated for a series of offset 'bar magnets', shown in the schematic diagram to the right. The black regions denote the ferromagnet. Note the aspect ratio of the roughness is different for presentational purposes. Right: Schematic diagram of the 'bar magnet' roughness. The yellow and light blue regions represent areas of positive and negative dipolar fields (aligned and opposed to the applied magnetic field). Also shown are two pairs of muons with a particular implantation energy (E_1 and E_2). The muons can experience either positive or negative dipolar fields, depending on their lateral (y) position. The hatched regions, labelled 1 and 2, correspond to the regions used in the summation in Figure 4.2.

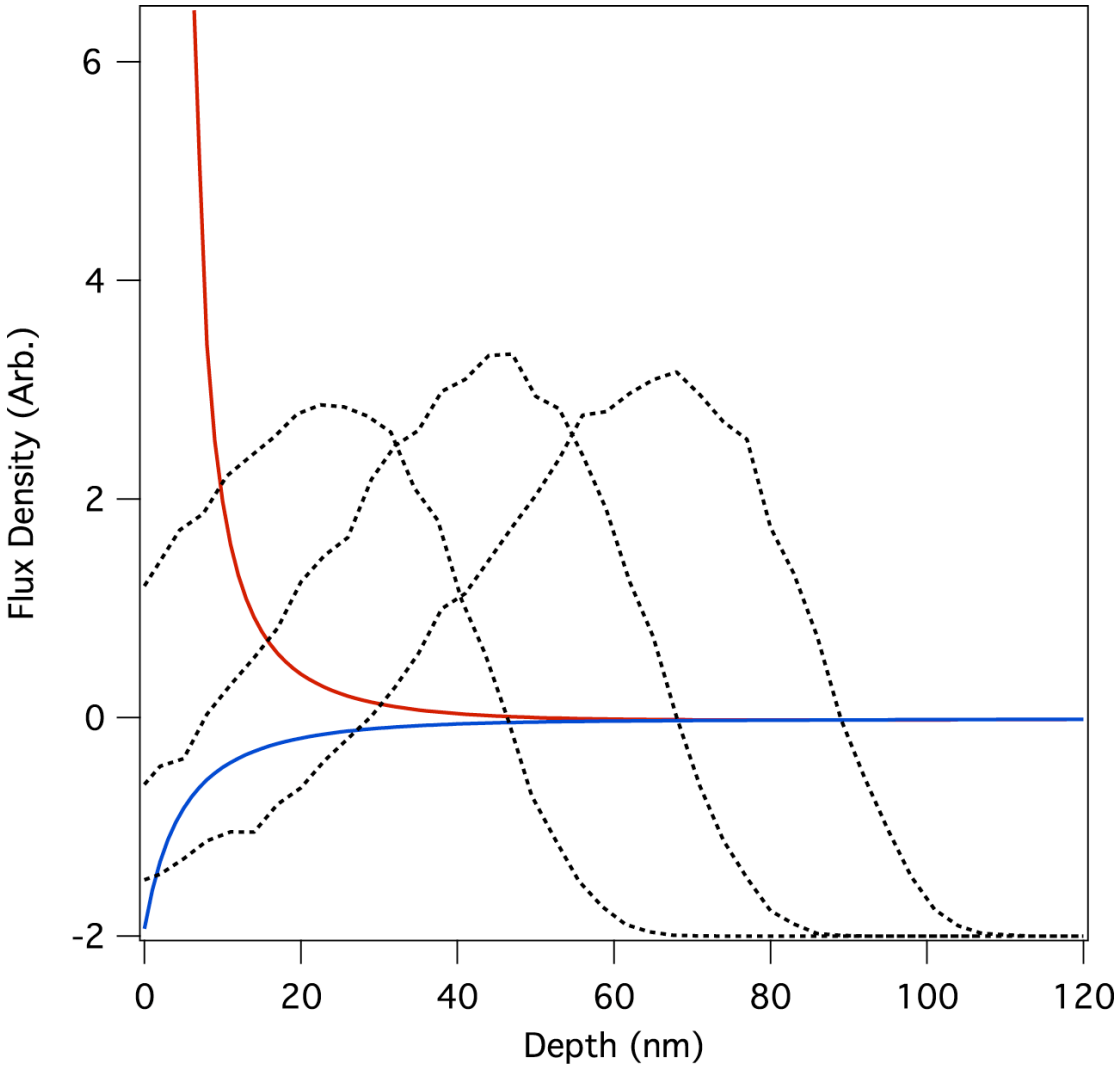

Figure 4.2: The sum (over y direction, normalised to area) of dipolar fields the muons experience inside the organic, calculated for the same model as shown in Figure 4.1 but with more realistic aspect ratio: pillars of 25 nm width and 2 nm height. Red: the sum of the flux density in the region extending from 'between' the pillars, designated by region 1 in Figure 4.1; Blue: the sum of the flux density in the region extending from 'above' the pillar, designated by region 2 in Figure 4.1. Apart from at very small distances, the dipolar fields have an approximately exponential decay from the interface. When comparing this to the depth profiles for the different energies (shown in black), it is apparent that the net magnetic field that the muon experiences is positive, explaining the positive skewness to our lineshapes.

We must therefore calculate a realistic dipolar field distribution in our sample in order to extract information about the spin injection. We use a model for the dipolar fields initially introduced to describe Fe / Cr / Fe thin film interlayer coupling [1]. It was shown that for a square lattice structure, at a given distance z from the interface of a rough FM, the dipolar field decays exponentially from the plane and can be approximated by a series of exponential terms [2]. This approximation significantly reduces the computational time required to calculate dipolar fields. The model is dependent on three parameters from each layer - the period of the roughness L, the magnetic moment per unit cell of the FM μ_M and the step height d – making a total of 6 for both layers. Since the dipolar fields are dominated by the smaller lateral dimension, we are able to extract the parameters from our characterisation data (L=25nm and d=1.5nm from the AFM and X-rays, and the magnetic moment from each layer from the magnetisation measurements). The results, shown in Figure 2 of the paper, are in extremely good agreement with the frequency domain data. Whilst there are clearly assumptions in our analysis that may not be valid, because of this agreement between model and data, we are satisfied that dipolar fields offer an adequate explanation of our data. This model was only used in the frequency domain analysis; time domain analysis is dealt with in Section 2 of this document.

References

[1] S. Demokritov *et al*., Phys. Rev. B 49, 720 (1994)

[2] B. Heinrich *et al*., Phys. Rev. B 38, 12879 (1988)